

BCSJ Award Article

One-Pot Synthesis of Soluble Precursors Possessing Both Al–N and B–N Backbones and Their Pyrolysis

Yusuke Mori and Yoshiyuki Sugahara*

Department of Applied Chemistry, School of Science and Engineering, Waseda University, 3-4-1 Ohkubo, Shinjuku-ku, Tokyo 169-8555

Received March 7, 2006; E-mail: ys6546@waseda.jp

Soluble precursors possessing both Al–N and B–N backbones have been prepared from $LiAlH_4$, $LiBH_4$, and $RNH_2 \cdot HCl$ (R = Me and Et) in one pot. The infrared (IR) and nuclear magnetic resonance (NMR) spectra of the precursors indicate that the precursors possess Al–H and B–H groups as well as Al–N, B–N, Al–(μ-H)$_2$–Al, and Al–(μ-H)$_2$–B bonds. TG analysis reveals that the ceramic yield of the precursor [**AB11_Me** ($LiAlH_4/LiBH_4/MeNH_2 \cdot HCl = 1/1/2$)] up to 1000 °C under an argon atmosphere is 74.4 mass %. The transmission electron microscopic (TEM) images and the X-ray diffraction (XRD) pattern of **AB11_Me** that was pyrolyzed at 1600 °C indicate that the average size of crystalline aluminum nitride (AlN) is about 14 nm and that crystalline AlN particles are distributed homogeneously in an amorphous matrix.

Pyrolytic conversion of precursors, so-called preceramic materials, is a chemical route to obtaining non-oxide ceramics and ceramic-based composites.[1–4] Using this approach, high-purity materials with a homogeneous distribution of component elements on an atomic scale and a controllable microstructure can be obtained at relatively low temperatures. When preceramic materials are fusible at relatively low temperatures or soluble in common organic solvents, this process can also offer fabrication routes to desirable shapes, including coatings and fibers, which are essentially unattainable by a conventional powder process.[4]

Aluminum nitride (AlN)–boron nitride (BN) composites possess many attractive properties, including high thermal conductivity and high electrical insulation as well as excellent machinability and lubricativity.[5–10] These properties suit them various applications,[5,7] such as electromagnetic window materials, heat sinks, and protective coatings of communication and detection equipment on aircraft. AlN–BN composites are generally prepared by a conventional powder process.[11–15] The powder process generally results in substantial anisotropy in their microstructures, however, and, consequently, in their various properties.[11]

Recently, a few studies have reported the preparation of AlN–BN ceramic-based composites by pyrolytic conversion of precursors. In an approach using metalorganic compounds, the precursors were synthesized by the reaction between $(Et_2AlNH_2)_3$ and $B(NEt)_3$ to form homogeneous composites composed of crystalline AlN and turbostatic-BN by pyrolysis.[5] In another approach, gels for AlN–BN composites were prepared by the ammonolysis of H_3BO_3, $AlCl_3$, and $(NH_2)_2CO$ in aqueous solutions.[16] As a one-pot synthesis approach, Dou et al. prepared precursors by reacting metal hydrides ($H_3Al \cdot NMe_3$ and $H_3B \cdot NH_3$) with ammonia.[17] Although homogeneously dispersed AlN–BN composites were considered to be obtained by this approach, all of these precursors were insoluble in common organic solvents.

Here, we report a one-pot synthesis of soluble precursors by the reactions involving lithium tetrahydridoaluminate ($LiAlH_4$), lithium tetrahydroborate ($LiBH_4$), and alkylamine hydrochloride ($RNH_2 \cdot HCl$; R = Me and Et). AlN precursors with Al–N backbones can be directly synthesized from $LiAlH_4$ and alkylamine hydrochlorides,[18] while borazines [$(HBNR)_3$; R = H or alkyl] can be prepared from sodium tetrahydroborate ($NaBH_4$) and alkylamine hydrochlorides ($RNH_2 \cdot HCl$) [or ammonium chloride (NH_4Cl)].[19]

$$n\mathrm{LiAlH_4} + n\mathrm{RNH_2 \cdot HCl} \rightarrow (\mathrm{HAlNR})_n + n\mathrm{LiCl} + 3n\mathrm{H_2}\ (\mathrm{R} = \text{alkyl}), \quad (1)$$

$$3\mathrm{NaBH_4} + 3\mathrm{RNH_2 \cdot HCl} \rightarrow (\mathrm{HBNR})_3 + 3\mathrm{NaCl} + 9\mathrm{H_2}\ (\mathrm{R} = \text{H or alkyl}), \quad (2)$$

Thus, it is expected that a precursor possessing both Al–N and B–N backbones can be directly synthesized from $LiAlH_4$, $LiBH_4$, and alkylamine hydrochlorides. In this study, we aim at the preparation of soluble precursors in one pot and their conversion into homogeneous composites with high ceramic yields. We report the preparation of precursors, the mechanism of the pyrolytic conversion and the characterization of the pyrolyzed residues.

Published on the web November 9, 2006; doi:10.1246/bcsj.79.1681

Table 1. The Precursors Prepared by Reactions of $LiAlH_4$, $LiBH_4$ with Methylamine Hydrochloride, and/or Ethylamine Hydrochloride

Sample	$LiAlH_4/LiBH_4/CH_3NH_2\cdot HCl/C_2H_5NH_2\cdot HCl$ (molar ratio)	Notes
AB11_Me	1/1/2/0	white solid, soluble
AB11_MeEt	1/1/1/1	white viscous liquid, soluble
AB11_Et	1/1/0/2	transparent viscous liquid, soluble

Experimental

All the manipulations were performed under protective nitrogen atmosphere (purity: >99.9995%) using standard Schlenk techniques[20] or a nitrogen-filled glove box. Toluene (Kanto Chemical) was distilled over sodium and benzophenone under nitrogen atmosphere.

Preparation of the Precursors. The precursors were synthesized by the reactions of lithium tetrahydridoaluminate ($LiAlH_4$, Wako Pure Chemical Industries) and lithium tetrahydroborate ($LiBH_4$, Wako Pure Chemical Industries) with methylamine hydrochloride ($CH_3NH_2\cdot HCl$, Tokyo Kasei Kogyo) and/or ethylamine hydrochloride ($C_2H_5NH_2\cdot HCl$, Tokyo Kasei Kogyo). The molar ratios in the preparation of precursors are listed in Table 1.

The preparation of **AB11_Me** is described below as a representative example, since the other precursors were prepared in a similar manner. The reaction was conducted in a three-necked round-bottomed flask equipped with a gas inlet tube, a glass stopper, and a reflux condenser. In a glove box, $LiAlH_4$ (4.212 g, 0.111 mol) and $LiBH_4$ (2.418 g, 0.111 mol) were added to the flask. After it was carefully purged with nitrogen, the apparatus was charged with distilled toluene. Methylamine hydrochloride (14.98 g, 0.222 mol) was dried under reduced pressure for 3 h and added to this suspension. The resulting suspension was stirred overnight at 0 °C and then gradually heated to 110 °C. After stirring at 110 °C for 16 h, the suspension was filtered to remove insoluble components. Toluene was removed from the clear solution by trap-to-trap distillation under reduced pressure to yield a white soluble solid [Caution: The precursors react vigorously with water to emit flammable (or toxic) gases (such as hydrogen, ammonia, etc.). Thus, the precursors should be kept under an inert atmosphere.].

Pyrolysis of the Precursor AB11_Me. For pyrolysis at 1600 °C, the precursor **AB11_Me** was placed on a BN boat in an alumina tube under flowing argon (purity: >99.999%). The heating rate was 10 °C min^{-1} from room temperature to 200 °C and 5 °C min^{-1} from 200 to 1600 °C. The temperature was held at 1600 °C for 2 h. The pyrolyzed residue was then cooled to room temperature at 5 °C min^{-1}.

Characterization of the Precursors and the Residue Pyrolyzed at 1600 °C. The precursors were characterized by infrared (IR) spectroscopy (JASCO, FT/IR-460) and nuclear magnetic resonance (NMR) spectroscopy (JEOL, JNM-Lambda 500). The IR spectra of the precursors (except for **AB11_Et**) were recorded using the hexachloro-1,3-butadiene (C_4Cl_6; hcb) mull technique. The ^{11}B NMR (160.35 MHz) spectra of the precursors were recorded for a benzene-d_6 solution using diethyl ether–boron trifluoride (1/1) ($BF_3\cdot Et_2O$, 0 ppm) as an external standard. The ^{27}Al NMR (130.20 MHz) spectra of the precursors were recorded using $[Al(H_2O)_6]^{3+}$ (0 ppm) as an external standard. Thermogravimetry (TG, Perkin-Elmer, TGA-7) was carried out at a heating rate of 10 °C min^{-1} under flowing argon (90 mL/min) up to 1000 °C. TG-mass spectrometry (MS, ANELVA, M-400GA-DM) analysis under flowing helium (40 mL min^{-1}, purity: >99.9999%) was performed in the range from 10 to 400 amu for the detection of the volatile species during pyrolysis. No fragments larger than 125 amu were observed.

The residue of **AB11_Me** that was pyrolyzed at 1600 °C was characterized by solid-state NMR spectroscopy (JEOL, NM-GSX 400), Raman spectroscopy (Thermo Electron, Nicolet Almega XR) and X-ray diffraction (XRD, Rigaku, Rint-2500) analysis. The solid-state NMR spectrum of the pyrolyzed residue was recorded at 128.28 MHz (^{11}B) and 104.17 MHz (^{27}Al) using only the MAS technique. The external standards for solid-state ^{11}B and ^{27}Al NMR were the same compounds as for liquid-state NMR. Five hundred scans were accumulated with a pulse delay of 5 s (^{11}B) or 1 s (^{27}Al) and a spinning rate of 9 kHz (^{11}B and ^{27}Al).

The X-ray diffraction pattern of the pyrolyzed residue was obtained using monochromated Cu Kα radiation. Microstructure characterization of the pyrolyzed residue was performed with a transmission electron microscope (TEM, JEOL, JEM-1011, 100 kV). The amounts of aluminum and boron in the precursor and the pyrolyzed residue were determined using inductively coupled plasma emission (ICP) spectrometry (Variant, Vista-MPX). The amounts of carbon, nitrogen and hydrogen in the precursor were measured with a Perkin-Elmer PE 2400-II instrument, and those of carbon, nitrogen and oxygen in the residue obtained by pyrolysis at 1600 °C were measured with LECO CS-444LS and TC-436 instruments.

Results and Discussion

TG curves of the precursors performed under flowing argon are shown in Fig. 1. The ceramic yields of **AB11_Me**, **AB11_MeEt**, and **AB11_Et** up to 1000 °C are 74.4, 68.5, and 39.1 mass %, respectively. Since **AB11_Me** exhibits the highest ceramic yield among these precursors, most of the study was devoted to the spectroscopic characterization of the precursor **AB11_Me** and its pyrolyzed residue.

Spectroscopic Characterizations of the Precursors. Figure 2 shows the IR spectrum of **AB11_Me**. The IR spectrum exhibits adsorption bands at 3245 cm^{-1} (ν_{NH}),[21]

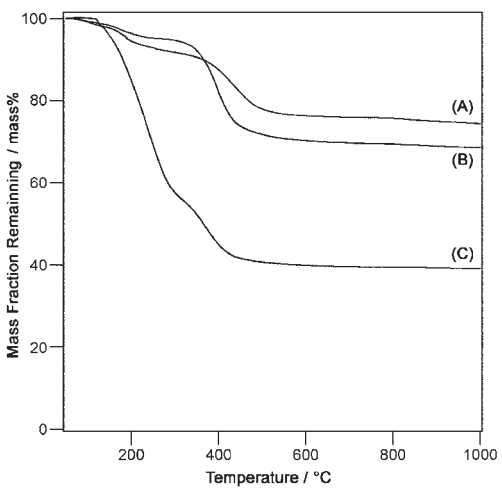

Fig. 1. TG curves of (A) **AB11_Me**, (B) **AB11_MeEt**, and (C) **AB11_Et** under flowing argon.

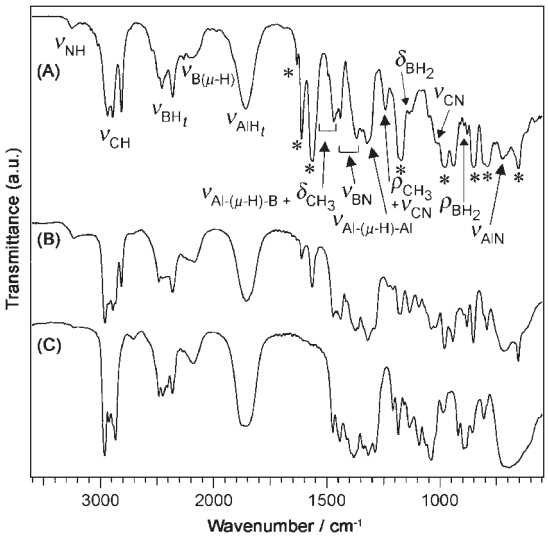

Fig. 2. IR spectra of (A) **AB11_Me**, (B) **AB11_MeEt**, and (C) **AB11_Et**. The bands marked by asterisks are due to hexachloro-1,3-butadiene (hcb).

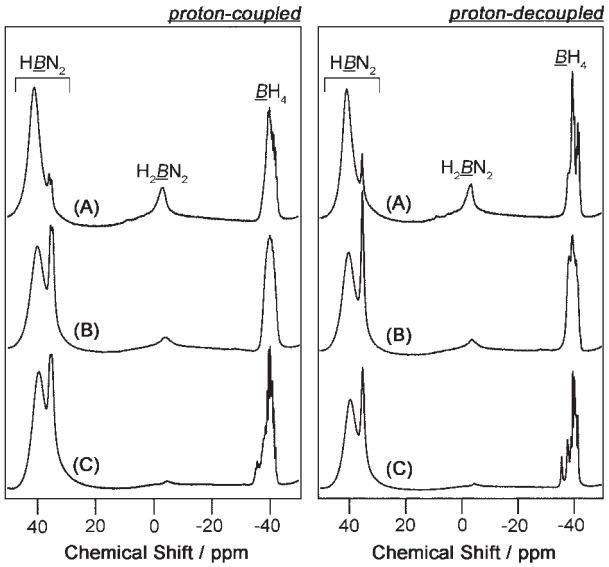

Fig. 3. Proton-coupled and decoupled ^{11}B NMR spectra of (A) **AB11_Me**, (B) **AB11_MeEt**, and (C) **AB11_Et**.

2960–2860 cm^{-1} (ν_{CH}),[21] 2480–2360 cm^{-1} (ν_{BH_t}),[22,23] 2180 cm^{-1} ($\nu_{B(\mu\text{-}H)}$),[22,23] 1860 cm^{-1} (ν_{AlH_t}),[18] 1490–1470 cm^{-1} ($\nu_{Al\text{-}(\mu\text{-}H)\text{-}B} + \delta_{CH_3}$),[22] 1460 and 1380 cm^{-1} (ν_{BN}),[19,21] 1320 cm^{-1} ($\nu_{Al\text{-}(\mu\text{-}H)\text{-}Al}$),[22] 1240 cm^{-1} ($\rho_{CH_3} + \nu_{CN}$),[21] 1123 cm^{-1} ($\delta_{BH_2}$),[22] 1020 cm^{-1} ($\nu_{CN}$),[21] 878 cm^{-1} ($\rho_{BH_2}$),[22] and ≈725 cm^{-1} (ν_{AlN})[24] (H_t donates the terminal hydrogen atom). This result indicates that **AB11_Me** possesses Al–H and B–H groups, and Al–N and B–N bonds as well as Al–H–B and Al–H–Al bridging bonds.

To characterize the molecular structures of the precursors further, multi-nuclear liquid-state NMR analysis was employed. Figure 3 shows both the proton-coupled and the decoupled ^{11}B NMR spectra of **AB11_Me**. In Fig. 3, four signals are present at 41, 35, −3, and ≈ −38 ppm. The signal at 35 ppm, which is a doublet in the proton-coupled spectrum and a singlet in the decoupled spectrum, can be assigned to an H*B*N$_2$ environment.[25] The coupling constant (J_{BH}) of this signal is 131 Hz. From the ^{11}B NMR spectra of borazines [(HBNR)$_3$; R = H or alkyl], *B*-alkenylborazines [(RCH=CH$_2$)–B$_3$N$_3$H$_5$; R = alkyl] and their polymerized compounds possessing a [B$_3$N$_3$] ring, the coupling constants (J_{BH}) of the H*B*N$_2$ resonances were determined to be 130–140 Hz.[19,25–27] Thus, the signal at 35 ppm in the ^{11}B NMR spectrum of **AB11_Me** is attributed to the H*B*N$_2$ environment in the [B$_3$N$_3$] ring.

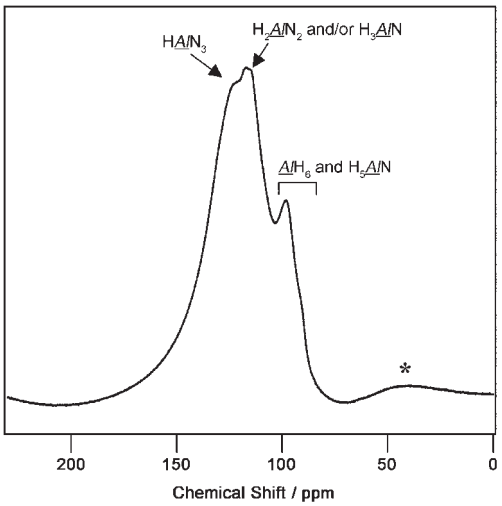

Fig. 4. ^{27}Al NMR spectrum of **AB11_Me**. The signal marked by an asterisk is caused by the glass tube.

As for the assignment of the broad signal centered at 41 ppm, the chemical shift in this range can be generally assigned to the H*B*N$_2$ environment.[25] This broad signal is a singlet in the proton-coupled spectrum, however, and thus it should not correspond to a usual H*B*N$_2$ environment. Bulak et al.[28] reported that the ^{11}B NMR spectra of the compounds possessing an [–N=B(H)–] skeleton exhibited barely resolved doublet signals at 39–41 ppm in the proton-coupled spectra in spite of the existence of the B–H groups. The line width of the signal, which can be assigned to the H*B*N$_2$ environment in the [–N=B(H)–] skeleton, in the decoupled spectrum was still broad in comparison with the width in the proton-coupled spectrum.[29] In Fig. 3, the broad signals at 41 ppm in the proton-coupled and decoupled spectra are singlets and the line widths of the signals are very similar to each other. Thus, it is concluded that the signal at 41 ppm corresponds to the H*B*N$_2$ environment in the [–N=B(H)–] skeleton. In addition, the broad signals centered at −3 ppm and at ≈ −38 ppm in the ^{11}B NMR spectrum of **AB11_Me** can be assigned to the H$_2$*B*N$_2$ and *B*H$_4$ environments.[22,25]

Figure 4 shows the ^{27}Al NMR spectrum of **AB11_Me**. Signals are observed at ≈124, 114–118, and 97 ppm with one shoulder at ≈91 ppm. With respect to the signals in the range from 114 to 118 ppm, Akitt reported that the chemical shifts from 116 to 120 could be assigned to the H$_2$*Al*N$_2$ and H$_3$*Al*N environments.[30] It is therefore suggested that the signals in the range from 114 to 118 ppm are assignable to the H$_2$*Al*N$_2$ and/or H$_3$*Al*N environments. The signal at ≈124 ppm is assignable to the H*Al*N$_3$ environment.[31] The signal at 97 ppm and the shoulder at ≈91 ppm in the ^{27}Al NMR spectrum of **AB11_Me** can be assigned to the six-coordinate *Al*H$_6$ and H$_5$*Al*N environments.[22]

Table 2. The Compositions of **AB11_Me** and the Residue Pyrolyzed at 1600 °C

Sample	Elemental analysis/mass %							Compositional formula
	Al	B	N	C	H	O	Total	
AB11_Me	27.9	8.5	26.0	28.2	8.4	—	99.0	$AlB_{0.77}N_{1.80}C_{2.28}H_{8.05}$
Calc.(**AB11_Me**)	27.6	11.0	28.6	24.5	8.2	—	100.0	$AlBN_2C_2H_8$
1600 °C	52.0	5.0	21.7	13.4	—	5.6	97.7	$AlB_{0.24}N_{0.80}C_{0.58}O_{0.18}$

The aluminum tetrahydroborate derivatives, such as $Al(BH_4)_3$ and $(\equiv N)\cdot HAl(BH_4)_2$, possess six-coordinate aluminum atoms and Al–(μ-H)$_2$–B bonds.[22] $Al(BH_4)_3$ has three Al–(μ-H)$_2$–B bonds in the six-coordinate AlH_6 environment, which exhibited a resonance at 97.4 ppm in the ^{27}Al NMR spectrum.[22] The derivative $(\equiv N)\cdot HAl(BH_4)_2$, on the contrary, has two Al–(μ-H)$_2$–B bonds in the six-coordinate H_5AlN environment, whose resonance appeared at 94.1 ppm in the ^{27}Al NMR spectrum.[22] The ^{11}B NMR spectra of both derivatives exhibited BH_4 resonances at ≈ -37 ppm.[22,25] **AB11_Me** correspondingly exhibits the signals at ≈ -38 ppm in the ^{11}B NMR spectrum and the signal at 97 ppm and the shoulder at $\approx$91 ppm in the ^{27}Al NMR spectrum. In addition, the $\nu_{Al-(\mu-H)-B}$ band is observed at 1490–1470 cm^{-1} in the IR spectrum of **AB11_Me**. Thus, it is suggested that **AB11_Me** contains the Al-$(BH_4)_3$ and $(\equiv N)\cdot HAl(BH_4)_2$ groups possessing Al–(μ-H)$_2$–B bonds.

The ^{27}Al NMR spectrum of **AB11_Me** suggests the presence of the four-coordinated aluminum species [H_xAlN_{4-x} (x = 1–3)] groups possessing Al–H groups. Since the $\nu_{Al-(\mu-H)-Al}$ band is observed at 1320 cm^{-1}, single hydrogen bridges [i.e., Al–(μ-H)–Al bonds] and/or double hydrogen bridges [i.e., Al–(μ-H)$_2$–Al bonds][22] could be present in **AB11_Me**. For the Al–(μ-H)–Al bonds, the adsorption band at 1200 cm^{-1}, as well as that at 1320 cm^{-1}, should be observed,[22] while no adsorption band at 1200 cm^{-1} is observed in the IR spectrum of **AB11_Me**. Thus, it is likely that only the Al–(μ-H)$_2$–Al bonds are present in **AB11_Me**. It should be noted that the Al–(μ-H)$_2$–Al bonds in **AB11_Me** can be located at both the six-coordinate Al environments (AlH_6 and H_5AlN) and/or the four-coordinate Al environments [H_xAlN_{4-x} (x = 2, 3)], but the formation of Al–(μ-H)$_2$–Al bonds at the AlH_6 and H_5AlN environments could hardly occur.[22] Based on these considerations, it is reasonable to assume the presence of Al–(μ-H)$_2$–Al bonds in the H_xAlN_{4-x} (x = 2, 3) environments.

Table 2 shows the composition of **AB11_Me**. As shown in Table 2, the boron/aluminum ratio was determined to be 0.77 by an ICP measurement. The boron content decreased during the preparation of **AB11_Me**, indicating that the volatile *N*-methylborazine $(HBNMe)_3$, which was identified by the ^{11}B NMR spectrum of the distillate (not shown), was formed by reaction of $LiBH_4$ with $MeNH_2\cdot HCl$. The average mass of **AB11_Me** was about 1.4×10^3 as determined by cryoscopy. Based on these observations, the local structure of **AB11_Me** can be proposed as illustrated in Fig. 5.

The molecular structures of **AB11_MeEt** and **AB11_Et** are also discussed on the basis of the spectroscopic results. All of the IR spectra exhibit similar adsorption bands, as shown in Fig. 2. Additionally, as shown in Fig. 3, the ^{11}B NMR spectra of **AB11_MeEt** and **AB11_Et** exhibit profiles similar to that of **AB11_Me**. Based on these observations, **AB11_Me**, **AB11_MeEt**, and **AB11_Et** appear to possess similar local environments.

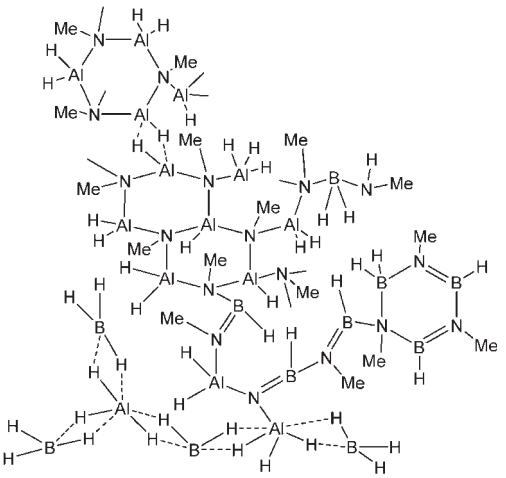

Fig. 5. The local structure of **AB11_Me**. Formal cherges on B, Al, and N atoms are omitted for clarity in this figure.

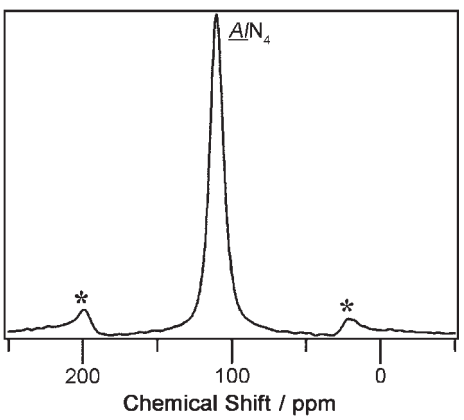

Fig. 6. Solid-state ^{27}Al NMR spectrum of **AB11_Me** pyrolyzed at 1600 °C. Spinning side bands are marked with asterisks.

Characterizations of the Residue Obtained by Pyrolysis at 1600 °C. The residue of **AB11_Me** that was pyrolyzed at 1600 °C was characterized by solid-state NMR spectroscopy, Raman spectroscopy, XRD, TEM, ED, and elemental analysis. Table 2 summarizes the compositions of the precursor **AB11_Me** and its pyrolyzed residue. The formula of the residue is $AlB_{0.24}N_{0.80}C_{0.58}O_{0.18}$. Figures 6 and 7 show the solid-state ^{27}Al and ^{11}B NMR spectra of the pyrolyzed residue, respectively. The solid-state ^{27}Al NMR spectrum of the residue shows one narrow signal at 110 ppm, which can be assigned to the AlN_4 environment.[32] In the solid-state ^{11}B NMR spectrum of the residue (Fig. 7), two broad signals centered at 11

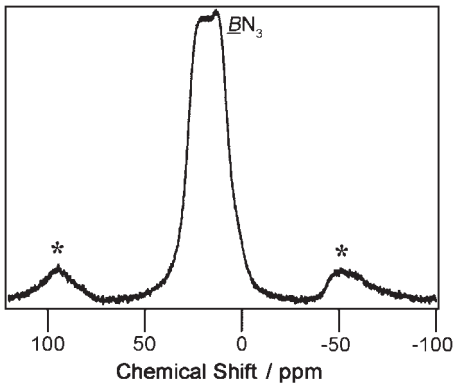

Fig. 7. Solid-state ^{11}B NMR spectrum of **AB11_Me** pyrolyzed at 1600 °C. Spinning side bands are marked with asterisks.

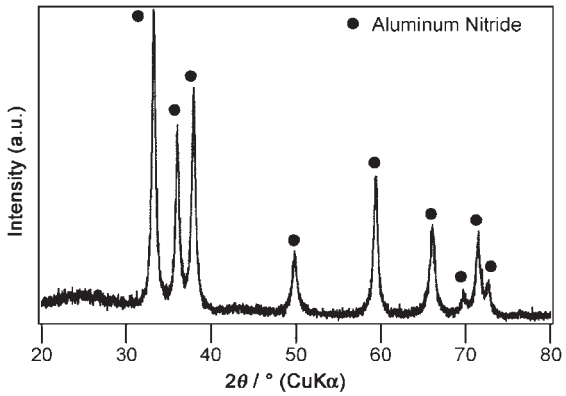

Fig. 8. XRD pattern of **AB11_Me** pyrolyzed at 1600 °C.

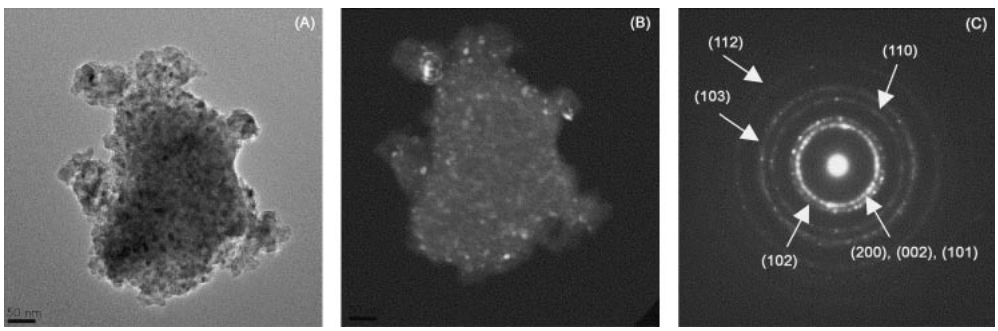

Fig. 9. TEM images [(A) bright-field image and (B) dark-field image] and (C) the ED pattern of **AB11_Me** pyrolyzed at 1600 °C.

and 22 ppm are observed, which can be assigned to the BN_3 environment.[33] The Raman spectrum of the residue exhibits two bands at 1337 and 1595 cm^{-1}, which are attributable to amorphous carbon.[34,35] Figure 8 shows the XRD pattern of the pyrolyzed residue. The XRD pattern of the residue is consistent with that of crystalline AlN,[36] and no reflection due to crystalline BN phase is observed. The average size of the crystalline AlN particles is calculated as approximately 13 nm by Scherrer's formula.

Although the BN_3 resonance is observed in the solid-state ^{11}B NMR spectrum, no reflection of crystalline BN is observed. In addition, the presence of amorphous carbon in the residue is detected by Raman spectroscopy. Thus, the amorphous phase seems to contain boron, nitrogen, and carbon. On the contrary, the only crystalline phase in the residue is AlN, judging from the XRD result. As shown in Table 2, the N:Al ratio is 0.80:1, whereas the N:Al ratio in crystalline AlN is 1:1. If all of aluminum in the residue was present as crystalline AlN, the amount of nitrogen in the residue would not be sufficient. Even if all of nitrogen in the residue was present in the crystalline AlN and aluminum was present as both AlN and alumina (Al_2O_3), latter of which has an Al:O ratio of 1:1.5, the amount of oxygen would not be sufficient. Thus, the amorphous phase should possess a certain amount of aluminum, as well as boron, nitrogen, carbon, and oxygen. It is consequently assumed that the crystalline phase in the residue is AlN and that the amorphous phase in the residue is an Al–B–N–C–O material. It should be noted that, in the solid-state ^{11}B and ^{27}Al NMR spectra, it appears to be difficult to observe weak signals of asymmetric environments related to amorphous oxynitrides, possibly N_xBO_{3-x} ($x = 1, 2$), N_xBO_{4-x} ($x = 1$–3) and/or N_xAlO_{4-x} ($x = 1$–3) environments, because both boron and aluminum are quadrupolar nuclei.

Figure 9 shows the TEM images and the electron diffraction (ED) pattern of the residue obtained by pyrolysis at 1600 °C. The selected ED pattern of the residue [Fig. 9C] in the bright-field image [Fig. 9A] shows ring patterns, which can be assigned to that of AlN. The bright area in the dark-field image [Fig. 9B] corresponds closely to the dark area in the bright-field image. The dark area in the bright-field image, consequently, corresponds to crystalline AlN particles, which are dispersed homogeneously in an amorphous matrix. The average size of the crystalline particles is about 14 nm, which is in good agreement with the particle size calculated from the XRD pattern by Scherrer's formula.

Mechanistic Study of the Conversion of the Precursor AB11_Me into Ceramics. As shown in Table 2, the boron/aluminum ratio decreases from 0.77 in **AB11_Me** to 0.24 in the pyrolyzed residue. It is therefore assumed that a large portion of boron was volatilized during pyrolysis. In order to clarify this behavior, TG-MS analysis of **AB11_Me** was carried out.

Figure 10 shows the temperature profiles of the mass fragments. The pyrolytic process of **AB11_Me** can be divided into two stages (stage I: below 350 °C, stage II: above 350 °C). Figures 10A and 10B show the temperature profiles of the mass fragments recorded at stage I. As shown in Fig. 10A, in the temperature range from 150 to 350 °C, the temperature profile of the fragment at m/z 30 is similar to those of the fragments at m/z 31 and 28. These fragments can therefore be assigned to methylamine ($MeNH_2$). As shown in Fig. 10B,

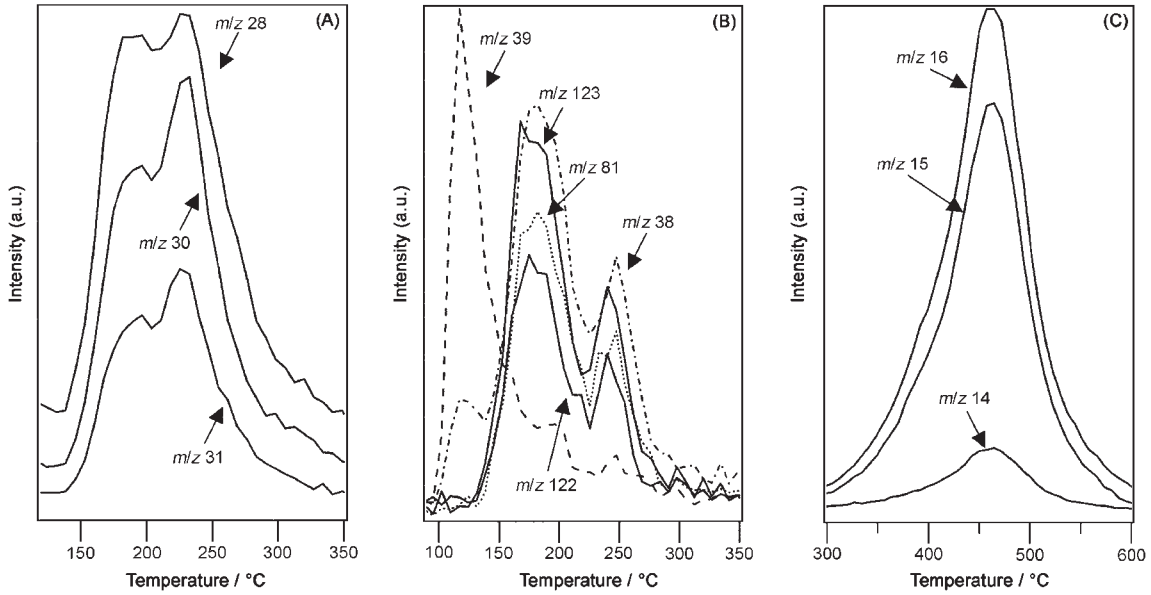

Fig. 10. Temperature profiles of fragments for (A) methylamine, (B) methylborazine and toluene, and (C) methane.

in the temperature range from 150 to 300 °C, the temperature profile of the fragment at m/z 123 is similar to those of the fragments at m/z 122, 81, and 38. These fragments can therefore be assigned to methylborazine $(HBNMe)_3$. Below 150 °C, the temperature profile of the fragment at m/z 38 is similar to that of the fragments at m/z 39, suggesting that these fragments are attributable to toluene. These observations suggest that toluene (below 150 °C), methylamine (150–350 °C), and methylborazine (150–300 °C) are evolved during pyrolysis. It is thus assumed that the evolution of methylborazine gives rise to the decrease in boron content.

Kim, Babonneau, and co-workers reported that evolution of borazine $(HBNH)_3$ was observed during the thermal decomposition of aminoborane polymer $(–H_2BNH_2–)_n$ possessing $[B_3N_3]$ rings in the temperature range from 200 to 330 °C.[37,38] Since **AB11_Me** also possess $[B_3N_3]$ rings, as shown in the ^{11}B NMR spectrum, it is assumed that cleavage of the B–N bonds occurs, leading to the evolution of methylborazine at this stage (Scheme 1A). On the other hand, Bernard et al. reported that the evolution of methylamine is due to the reaction between two –N(H)Me groups to form several =B–N(Me)–B= linkages during pyrolysis of poly[2,4,6-tri(methylamino)-borazine] below 400 °C[39] (Scheme 1B). The evolution of methylamine implies, therefore, that **AB11_Me** may contain –N(H)Me groups.

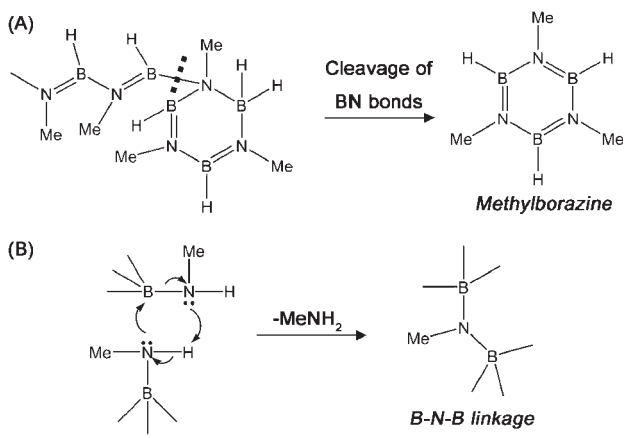

Scheme 1. Proposed reactions during pyrolysis of **AB11_Me** below 350 °C. Formal cherges on B, Al, and N atoms are omitted for clarity in this Scheme.

In Fig. 10C, which represents stage II, the temperature profile of the fragment at m/z 16 is similar to those of the fragments at m/z 15 and 14. These fragments can therefore be assigned to methane. In previous studies, the cleavage of the C–N bonds was reported to occur, leading to evolution of various hydrocarbons in this temperature range.[40–43] It is therefore assumed that the cleavage of the C–N bonds in the precursor leads to evolution of methane above 350 °C.

Conclusion

The soluble precursors have been synthesized from lithium tetrahydridoaluminate, lithium tetrahydroborate, and alkylamine hydrochloride in one pot. Spectroscopic analysis suggests that **AB11_Me** contains H_xAlN_{4-x} groups ($x = 1$–3), $Al(BH_4)_3$ groups, $(\equiv N)\cdot HAl(BH_4)_2$ groups, H_2BN_2 groups, and HBN_2 groups in the $[B_3N_3]$ ring. These units are likely to be connected via an [–N=B(H)–] skeleton as well as Al–(μ-H)$_2$–B and Al–(μ-H)$_2$–Al bridging bonds in **AB11_Me**. The other precursors, **AB11_MeEt** and **AB11_Et**, seem to have similar local environments, as suggested by IR and ^{11}B NMR. TG analysis exhibits that the ceramic yield of **AB11_Me** up to be 1000 °C under an argon atmosphere is 74.4 mass %. The decrease in the boron content during pyrolysis of **AB11_Me** arises from the evolution of methylborazine below 350 °C. The results of solid-state NMR, XRD, TEM, ED, and elemental analysis suggest that the residue of **AB11_Me** pyrolyzed at 1600 °C exhibits homogeneous distribution of crystalline AlN (≈14 nm) particles in the Al–B–N–C–O amorphous matrix. These results indicate that the one-pot synthesis involving $LiAlH_4$, $LiBH_4$, and $MeNH_2\cdot HCl$ is highly effective in fabricating precursors exhibiting high ceramic yields.

The authors gratefully thank Prof. Kazuyuki Kuroda, Department of Applied Chemistry at Waseda University, for his valuable discussion. This work is supported in part by Waseda university (special research project, 2000A-147) and 21COE "Practical Nano-Chemistry" from the MEXT, Japan.

References

1 K. J. Wynne, R. W. Rice, *Ann. Rev. Mater. Sci.* **1984**, *14*, 297.
2 G. Pouskouleli, *Ceram. Int.* **1989**, *15*, 213.
3 C. K. Narula, *Ceramic Precursor Technology and Its Applications*, Marcel Dekker, New York, **1995**.
4 J. Bill, F. Aldinger, *Adv. Mater.* **1995**, *7*, 775.
5 D. Kwon, W. R. Schmidt, L. V. Interrante, P. Marchetti, G. Maciel, *Inorganic and Organometallic Oligomer and Polymers*, ed. by J. F. Harrod, R. M. Laine, Kluwer Academic Publisher, Boston, MA, **1991**, pp. 191–197.
6 J. R. Morris, R. A. Tanzilli, U.S. Patent 4 666 873, **1987**.
7 K. S. Mazdiyasni, R. Ruh, E. E. Hermes, *Am. Ceram. Soc. Bull.* **1985**, *64*, 1149.
8 D. J. Twait, W. J. Lackey, A. W. Smith, W. Y. Lee, J. A. Hanigofsky, *J. Am. Ceram. Soc.* **1990**, *73*, 1510.
9 W. Y. Lee, W. J. Lackey, G. B. Freeman, P. K. Agrawal, D. J. Twait, *J. Am. Ceram. Soc.* **1990**, *74*, 2136.
10 S. Du, Z. Liu, L. Q. Gao, F. Li, L. T. Li, *Am. Ceram. Soc. Bull.* **1997**, *76*, 69.
11 T. Kanai, K. Tanemoto, H. Kubo, *Jpn. J. Appl. Phys., Part 1* **1990**, *29*, 683.
12 T. Kanai, A. Ando, K. Tanemoto, *Jpn. J. Appl. Phys., Part 1* **1992**, *31*, 1426.
13 T. Kanai, K. Tanemoto, *Jpn. J. Appl. Phys., Part 1* **1993**, *32*, 3544.
14 T. Kanai, T. Iseki, *J. Ceram. Soc. Jpn.* **1998**, *106*, 514.
15 G. J. Zhang, J. F. Yang, M. Ando, T. Ohji, *J. Am. Ceram. Soc.* **2002**, *85*, 2938.
16 T. D. Xiao, K. E. Gonsalves, P. R. Strutt, *J. Am. Ceram. Soc.* **1993**, *76*, 987.
17 D. Dou, D. R. Ketchum, E. J. M. Hamilton, P. A. Florian, P. J. Grandinetti, S. G. Shore, *Chem. Mater.* **1996**, *8*, 2839.
18 M. Cesari, S. Cucinella, *The Chemistry of Inorganic Homo- and Heterocycles*, ed. by D. B. Sowerby, I. Haiduc, Academic Press, London, **1987**, pp. 167–190.
19 O. T. Beachley, Jr., *Inorg. Chem.* **1969**, *8*, 981.
20 D. F. Shriver, M. A. Drezdzon, *The Manipulation of Air-Sensitive Compounds*, 2nd ed., Wiley-Interscience, New York, **1986**.
21 N. B. Colthup, L. H. Daly, S. E. Wiberley, *Introduction to Infrared and Raman Spectroscopy*, Academic Press, New York, **1964**.
22 A. J. Downs, L. A. Jones, *Polyhedron* **1994**, *13*, 2401.
23 J. O. Jansen, *Spectrochim. Acta, Part A* **2003**, *59*, 1565.
24 E. G. Brame, Jr., J. L. Margrave, V. W. Meloche, *J. Inorg. Nucl. Chem.* **1957**, *5*, 48.
25 H. Nöth, B. Wrackmeyer, *Nuclear Magnetic Resonance Spectroscopy of Boron Compounds*, Springer-Verlag, New York, **1978**.
26 A. T. Lynch, L. G. Sneddon, *J. Am. Chem. Soc.* **1989**, *111*, 6201.
27 P. J. Fazen, L. G. Sneddon, *Organometallics* **1994**, *13*, 2867.
28 E. Bulak, T. Varnali, P. Paetzold, U. Englert, *Z. Anorg. Allg. Chem.* **1999**, *625*, 3.
29 U. Braun, B. Böck, H. Nöth, I. Schwab, M. Schwartz, S. Weber, U. Wietelmann, *Eur. J. Inorg. Chem.* **2004**, 3612.
30 J. W. Akitt, *Prog. Nucl. Magn. Reson. Spectrosc.* **1989**, *21*, 1.
31 H. Nöth, P. Wolfgardt, *Z. Naturforsch., B: Chem. Sci.* **1976**, *31*, 697.
32 N. D. Butler, R. Dupree, M. H. Lewis, *J. Mater. Sci. Lett.* **1984**, *3*, 469.
33 P. S. Marchetti, D. Kwon, W. R. Schmidt, L. V. Interrante, G. E. Maciel, *Chem. Mater.* **1991**, *3*, 482.
34 S. Trassl, G. Motz, E. Rössler, G. Ziegler, *J. Am. Ceram. Soc.* **2002**, *85*, 239.
35 G. Gregori, H.-J. Kleebe, H. Brequel, S. Enzo, G. Ziegler, *J. Non-Cryst. Solids* **2005**, *351*, 1393.
36 The JCPDS file, No. 25-1133.
37 D. P. Kim, K. T. Moon, J. G. Kho, J. Economy, C. Gervais, F. Babonneau, *Polym. Adv. Technol.* **1999**, *10*, 702.
38 C. Gervais, F. Babonneau, *J. Organomet. Chem.* **2002**, *657*, 75.
39 S. Bernard, D. Cornu, P. Miele, H. Vincent, J. Bouix, *J. Organomet. Chem.* **2002**, *657*, 91.
40 G. T. Burns, T. P. Angelotti, L. F. Hanneman, G. Chandra, J. A. Moore, *J. Mater. Sci.* **1987**, *22*, 2609.
41 Y. Liu, D. R. Treadwell, M. R. Kannisto, B. L. Mueller, R. M. Laine, *J. Am. Ceram. Soc.* **1997**, *80*, 705.
42 Y. Saito, Y. Sugahara, K. Kuroda, *J. Am. Ceram. Soc.* **2000**, *83*, 2436.
43 S. Koyama, H. Takeda, T. Tsugoshi, K. Watari, Y. Sugahara, *J. Ceram. Soc. Jpn.* **2006**, *114*, 563.